

Inferring Coupled Stuart–Landau Equations from Waveforms

Yuki Araya,^{1,*} Hiroaki Ito,^{1,†} Hiroshi Kori,^{2,‡} and Hiroyuki Kitahata^{1,§}

¹*Department of Physics, Chiba University, Chiba 263-8522, Japan*

²*Graduate School of Frontier Sciences, The University of Tokyo, Chiba 277-8561, Japan*

(Dated: February 16, 2026)

We present a data-driven framework to infer phase–amplitude equations of coupled limit-cycle oscillators directly from waveform measurements. Exploiting the universality of the Stuart–Landau normal form near a supercritical Hopf bifurcation, we reconstruct a near-identity transformation from two independent observables of an isolated oscillator and infer the intrinsic Stuart–Landau parameters. Using this reconstructed transformation, we then estimate linear coupling coefficients from paired measurements. The method accurately recovers parameters for coupled van der Pol oscillators, providing a quantitative benchmark. Applied to a high-dimensional hydrodynamic system of two coupled collapsible-channel oscillators, the inferred Stuart–Landau model captures bistability between in-phase and anti-phase synchronization and reveals that the anti-phase state is destabilized through a Neimark–Sacker bifurcation. Our approach enables quantitative prediction of synchronization transitions involving amplitude dynamics from experimentally accessible waveform data.

Synchronization, the phenomenon in which self-sustaining oscillators adjust their rhythms through interaction, appears in various systems [1–4]. Examples include mechanical systems [5–7], chemical systems [8–10], cell populations [11] such as cardiac cells [12] and clock cells [13], and fluid interaction systems of flagella and cilia [14–16]. Synchronization is essential for the functioning of many artificial and biological systems.

Most oscillator populations, with some exceptions, are inherently high-dimensional systems. Nevertheless, low-dimensional dynamics often play a pivotal role in shaping collective behavior, even within such complex systems. As a result, reducing these systems to low-dimensional representations has been fundamental to the universal and unified understanding of synchronization phenomena. A prominent example is the phase reduction method [2, 4, 17]. This approach models each oscillator using a single variable, the phase, and provides a reliable approximation of the system’s dynamics when interactions and perturbations are sufficiently weak. Beyond theoretical insights, phase equations have been successfully applied to the design and control of synchronization patterns in complex systems [9, 18]. In recent years, considerable efforts have been made to infer phase equations directly from empirical data obtained from coupled oscillator systems [9, 19–23]. These data-driven approaches enable the extraction of key information, such as coupling structures, interaction strengths, noise levels, and network topology.

However, the dynamics of oscillatory systems cannot be fully captured by phase equations alone. Many phenomena critically depend on amplitude variations, including continuous transitions from damped oscillations to limit cycles via Hopf bifurcations, destabiliza-

tion of limit cycles through period-doubling or Neimark–Sacker bifurcations, and various routes to chaos [24]. To understand such phenomena, low-dimensional models known as complex amplitude equations or phase–amplitude equations are particularly useful. These equations can be systematically derived when the governing equations of the system are known [2, 25, 26]. In many real-world systems, however, the governing equations are unknown or difficult to obtain. Therefore, as with phase equations, estimating phase–amplitude equations directly from observational data is expected to advance our understanding of system dynamics and facilitate applications such as prediction and control.

For prediction tasks, recent developments in machine learning have enabled model-free approaches that do not rely on explicit mathematical formulations. Nonetheless, these methods often require large datasets, which may be impractical depending on the experimental context. Moreover, it remains an open question whether machine learning can truly enhance our conceptual understanding of the underlying dynamics.

In this study, we propose a methodology for estimating phase–amplitude equations for interacting oscillators near a supercritical Hopf bifurcation. In addition to enhancing our understanding of the underlying dynamics, we demonstrate that the estimated equations can be used for effective prediction. Specifically, we adopt the Stuart–Landau equation with linear interaction terms as the model for estimation. This choice is motivated by two key considerations: (i) the normal form theory ensures that oscillators near a supercritical Hopf bifurcation can be well approximated by the Stuart–Landau equation via a nonlinear transformation known as the near-identity transformation; and (ii) near such bifurcations, the oscillation amplitude remains small, making linear interactions dominant. Figure 1 provides an overview of the proposed method. First, we estimate the near-identity transformation that maps two independent time series, obtained from an isolated oscillator, into a system exhibiting rotational symmetry. Using the inferred

* araya.yuuki.work@gmail.com

† ito@chiba-u.jp

‡ kori@k.u-tokyo.ac.jp

§ kitahata@chiba-u.jp

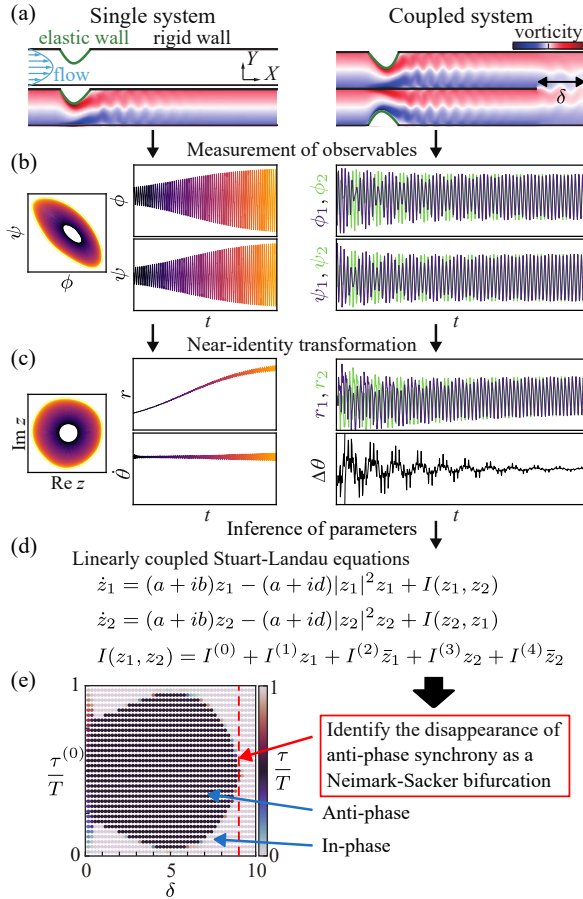


FIG. 1. Schematic overview of the proposed approach with data from a hydrodynamic system used for demonstration. (a) Snapshot of the hydrodynamic system. The system shows bistability between in-phase and anti-phase synchronization (see details in (e)). (b) Example time series $\phi(t)$ and $\psi(t)$, which can be arbitrarily chosen observables from the system. (c) Result of the optimal variable transformation, which maps the original variables (ϕ, ψ) to the rotation-symmetric coordinates $z = re^{i\theta}$, eliminating the dependence of amplitude and phase evolution on the intrinsic oscillation period. (d) The estimated model, in which the transformed variables in (c) are expected to follow in a good approximation. Colors indicate the time course in the panels (b) and (d). As will be shown in Fig. S3, analysis of the estimated model in (d) reveals that the loss of the anti-phase synchronized state occurs via a Neimark-Sacker bifurcation. (e) Color map that represents the final phase difference τ/T after transients in the plane spanned by the initial phase difference $\tau^{(0)}/T$ between the oscillators (vertical axis) and the coupling strength δ (horizontal axis), the system exhibits bistability between in-phase and anti-phase synchronization for small δ , while the anti-phase state disappears near $\delta \simeq 9$.

nonlinear transformation, we then estimate the parameters of the Stuart–Landau equation. Furthermore, by applying the same transformation to time series data from interacting oscillator systems, we can extract the interaction terms. We apply this methodology to two distinct systems. The first is a coupled van der Pol (VDP) os-

cillator system, which can be analytically reduced to the Stuart–Landau form and thus serves as a benchmark for validating our approach. The second is the model of a fluid system, chosen to demonstrate the applicability of our method to a far more complex system. Finally, we discuss the broader implications and future prospects of this research.

Our methodology assumes that time-series data can be obtained from two types of systems: (i) an isolated oscillator, from which we measure two observables, $\phi(t)$ and $\psi(t)$; and (ii) a pair of coupled oscillators, from which we measure four observables, $\phi_i(t)$ and $\psi_i(t)$ for $i = 1, 2$. The data from the isolated oscillator are used to infer the parameters of the nonlinear variable transformation and the Stuart–Landau equation. The data from the coupled oscillators are used to estimate the coupling terms.

We begin by describing the procedure for inferring the variable transformation and the parameters of the single Stuart–Landau equation. When the oscillator is near a supercritical Hopf bifurcation point, $\phi(t)$ and $\psi(t)$ may be parametrized in a good approximation by the complex variable $z(t)$ and its complex conjugate $\bar{z}(t)$ that obey the Stuart–Landau equation:

$$\dot{z} = (a + ib)z - (c + id)|z|^2z, \quad (1)$$

where a, b, c and d are real parameters. We fix $c = a > 0$ without loss of generality, as this corresponds to the linear transformation $z \rightarrow \sqrt{a/c}z$. Then, the amplitude of the stable limit cycle becomes unity and the oscillation period is given as $b - d$. Thus, we can determine $b - d$ from the oscillation period after a transient process. To infer a and d from $\phi(t)$ and $\psi(t)$, we consider a transformation $(\phi, \psi) \mapsto (z, \bar{z})$. This transformation is established in the method of normal forms [27, 28]. Specifically, we consider a combination of the linear transformation $(\phi, \psi) \mapsto (w, \bar{w})$ defined by

$$w = q_\phi\phi + q_\psi\psi - C^{(0,0)}, \quad (2)$$

where q_ϕ , q_ψ , and $C^{(m,n)}$ are complex parameters, and the nonlinear transformation $(w, \bar{w}) \mapsto (z, \bar{z})$ defined by

$$w = z + h_2(z, \bar{z}) + h_3(z, \bar{z}) + \mathcal{O}(4), \quad (3)$$

where $\mathcal{O}(4)$ expresses the higher-order terms $z^n\bar{z}^m$ with $n + m \geq 4$; h_2 and h_3 are second- and third-order polynomials described as

$$h_2(z, \bar{z}) = C^{(2,0)}z^2 + C^{(1,1)}z\bar{z} + C^{(0,2)}\bar{z}^2, \quad (4)$$

$$h_3(z, \bar{z}) = C^{(3,0)}z^3 + C^{(1,2)}z\bar{z}^2 + C^{(0,3)}\bar{z}^3. \quad (5)$$

The parameters q_ϕ , q_ψ , and $C^{(m,n)}$ except $C^{(1,1)}$ and $C^{(1,2)}$ are estimated using the Fourier series of $\phi(t)$ and $\psi(t)$ after the transient process. See Sect. I of Supplemental Material (SM) [29]. Taking the inverse of Eq. (3), we obtain

$$z = w - h_2 - h_3 + h_2 \frac{\partial h_2}{\partial w} + \bar{h}_2 \frac{\partial h_2}{\partial \bar{w}} + \mathcal{O}(4), \quad (6)$$

where all the terms except for w are functions of w and \bar{w} . Let $\hat{z}(t)$ be $z(t)$ obtained from $\phi(t)$ and $\psi(t)$ using Eqs. (2) and (6). We may now estimate indeterminate parameters by fitting $\hat{z}(t)$ to an analytical solution to an initial value problem for Eq. (1); i.e., $z = re^{i\theta}$ with $r = \left[1 + \left(\frac{1}{r_0^2} - 1\right)e^{-2at}\right]^{-\frac{1}{2}}$ and $\theta = (b-d)t + \frac{d}{a} \ln \frac{r}{r_0} + \theta_0$, where r_0 and θ_0 are real constants determined by the initial conditions. By numerically minimizing the cost function $F_{\text{cost}}^{(1)} = \frac{1}{t_w} \int_{t_s}^{t_s+t_w} |\hat{z} - z|^2 dt$, we obtain optimal values of $C^{(1,1)}$, $C^{(1,2)}$, a , d , r_0 , and θ_0 . Here, t_s and t_w are respectively the start and duration of the time series used for the inference, which are treated as hyperparameters optimized later.

Next, we infer the coupling between oscillators 1 and 2. We assume that the time evolution of z_k as

$$\dot{z}_k = G_k(z_k, z_\ell) = (a + ib)z_k - (a + id)|z_k|^2 z_k + I^{(0)} + I^{(1)}z_k + I^{(2)}\bar{z}_k + I^{(3)}z_\ell + I^{(4)}\bar{z}_\ell, \quad (7)$$

where $(k, \ell) = (1, 2)$ and $(2, 1)$, and $I^{(0)}$, $I^{(1)}$, $I^{(2)}$, $I^{(3)}$, and $I^{(4)}$ are complex constants. We include only linear terms for couplings because they are expected to be dominant in oscillators near the supercritical Hopf bifurcation. In detail, we compute $\hat{z}_k(t)$ from $\phi_k(t)$ and $\psi_k(t)$ by using Eqs. (2) and (6) along with parameters inferred from the isolated oscillator. The coupling parameters are then inferred by fitting $\hat{z}_1(t)$ and $\hat{z}_2(t)$ with various initial conditions to Eq. (7) by minimizing the cost function $F_{\text{cost}}^{(2)} = \sum_{\text{i.c.}} \frac{1}{t_w} \int_{t_s}^{t_s+t_w} \left(|\dot{\hat{z}}_1 - G_1(\hat{z}_1, \hat{z}_2)|^2 + |\dot{\hat{z}}_2 - G_2(\hat{z}_2, \hat{z}_1)|^2 \right) dt$ using a differential evolution method, where the summation is taken over the time series with different initial conditions specified later.

To achieve robust parameters for inference of the single and coupled Stuart-Landau equations, we systematically searched the optimal values of the start time t_s and the duration t_w . To evaluate the robustness of inference in the t_s - t_w space, we introduce the cost function

$$F_{\text{cost}}^{(\text{hyp})} = \left| \frac{\partial \mathbf{c}}{\partial t_s} \right|^2 + \left| \frac{\partial \mathbf{c}}{\partial t_w} \right|^2, \quad (8)$$

where the derivative denotes the forward difference and \mathbf{c} denotes the set of inferred parameters; $\mathbf{c} = (C^{(1,1)}, C^{(1,2)}, a, d)$ for the single system and $\mathbf{c} = (I^{(0)}, I^{(1)}, I^{(2)}, I^{(3)}, I^{(4)})$ for the coupled system. Hyperparameters t_s and t_w are selected from regions where $F_{\text{cost}}^{(\text{hyp})}$ remains consistently low.

We verify our proposed method using a low-dimensional oscillator model. Specifically, we employ the coupled VDP oscillators expressed as

$$\ddot{x}_k = (\mu - x_k^2)\dot{x}_k - x_k - I_x(x_k - x_\ell) - I_v(\dot{x}_k - \dot{x}_\ell), \quad (9)$$

where $x_{k,\ell}$ with $(k, \ell) = (1, 2)$ and $(2, 1)$ are real variables; μ , I_x , and I_v are real constants. For this model,

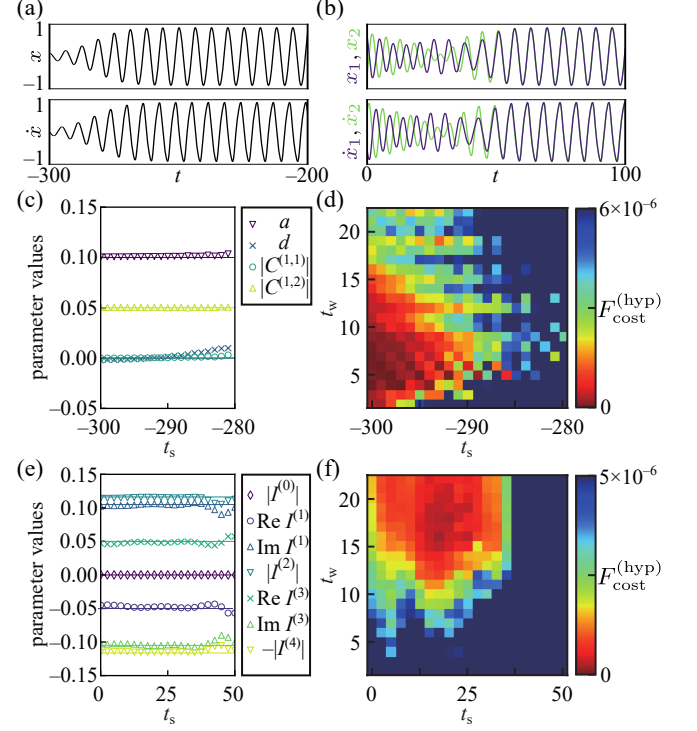


FIG. 2. Estimation results for the van der Pol (VDP) oscillator system. (a) Typical time series of x and \dot{x} used to infer the parameters of a single oscillator. (b) Typical time series of x_k and \dot{x}_k ($k = 1, 2$) used to infer the parameters of coupled oscillators. (c) Estimated parameters of a single oscillator plotted against different values of t_s at $t_w = 5$. (d) Stability diagram of the estimation in the t_s - t_w plane for the single oscillator. (e) Estimated interaction parameters between oscillators plotted against t_s at $t_w = 18$. (f) Stability diagram of the interaction parameter estimation in the t_s - t_w plane. In (c) and (e), symbols represent the estimated values, and solid lines indicate the theoretical values. In (d) and (f), regions with lower cost function values indicate higher estimation stability.

as detailed in Sect. II of SM [29], we obtain the following expressions to the lowest order of μ : $a = \mu/2$, $b = 1$, $d = 0$, $I^{(0)} = 0$, $I^{(3)} = -I^{(1)} = I_v/2 - i(2I_x + \mu I_v)/4$, $I^{(4)} = -I^{(2)}$, and $|I^{(2)}| = |I^{(1)}|$. The arguments of $I^{(2)}$ and $I^{(4)}$ are uniquely determined if the transformation between z_k and (x_k, \dot{x}_k) is fixed (see Sect. II in SM [29]). Stability boundaries in the (I_v, I_x) plane are obtained using these expressions (see Sect. III of SM [29]). There is a region of bistability of in-phase and anti-phase synchrony, which is surrounded by the pitchfork and the Neimark-Sacker bifurcation curves (see Fig. S1 in SM [29]).

We apply our method to Eq. (9), using $x_k(t)$ and $\dot{x}_k(t)$ as observables. An example of time series is shown in Figs. 2(a) and 2(b). For an isolated oscillator, we use a time series with an initial condition deviated from the limit cycle. For the coupled oscillator system, we generate time series data from a variety of initial conditions.

These initial conditions are constructed as follows. First, we extract a nearly periodic solution of a single oscillator after its transient phase, represented by $(x_p(t), \dot{x}_p(t))$ with $0 \leq t < T$, where T denotes the period of the solution. To scan the phase difference between two oscillators, we fix the initial condition of one oscillator at $(x_p(0), \dot{x}_p(0))$ and set the initial condition of the other oscillator to $(x_p(\tau^{(0)}), \dot{x}_p(\tau^{(0)}))$, where $\tau^{(0)}$ controls the phase offset. For VDP oscillators, $\tau^{(0)}$ is selected from 21 equally spaced points over the interval $[0, T]$. Details are shown in Sect. IV of SM [29].

As shown in Figs. 2(c) and 2(e), there are intervals of t_s and t_w in which the inferred quantities closely match the theoretical values, demonstrating the reliability of our methodology. Moreover, as shown in Figs. 2(d) and 2(f), such intervals coincide with the region in which $F_{\text{cost}}^{(\text{hyp})}$ is small, indicating the effectiveness of the cost function to determine the hyperparameters. It is also worth noting that, for the single system, an appropriate t_w is comparable to the transient time of the system, which is reasonable because the transient process contains global information about the system.

Next, we adopted the proposed method for two coupled oscillatory flows in two collapsible channels merging into a single channel (See Fig. 1(a)). When the softness of the elastic wall exceeds a critical threshold, oscillatory flow emerges in each channel via a supercritical Hopf bifurcation. In this study, we focus on the conditions slightly above this bifurcation point. The strength of the coupling between two channels is controlled by the distance δ between the merging point and the outlet [30]. For $\delta = 0$, the channels are independent. The details of hydrodynamic numerical simulation are shown in Sect. V of SM [29]. As shown in Fig. 1(e), the oscillatory flows can synchronize in-phase or anti-phase depending on the value of δ and the initial phase difference. We observe that the in-phase synchrony is possible for all the range of δ under consideration, whereas the anti-phase synchrony does not occur for $\delta > \delta_c$, where $\delta_c \simeq 9.0$ in the employed setup.

Next, we demonstrate that our inference method enables us to perform the stability analysis and clarify that the anti-phase synchrony is destabilized through a Neimark-Sacker bifurcation at $\delta = \delta_c$. We use the positions (X, Y) of the lowest part of the elastic wall as observables for each oscillator (see Fig. 1(a)). The initial conditions are constructed in the same manner as for the VDP oscillators, with $\tau^{(0)}$ selected from 30 equally spaced points over the interval $[0, T]$, where T denotes the period of the reference periodic solution. The details of inference are shown also in Sect. V of SM [29]. As shown in Fig. S2 in SM [29], our method successfully identifies hyperparameter regions where the inference remains consistently stable, demonstrating its reliability.

We perform linear stability analysis for the phase-amplitude equation given in Eq.(7) by neglecting the non-resonant terms $I^{(0)}$, $I^{(2)}\bar{z}_k$, and $I^{(4)}\bar{z}_\ell$ (see Sect. III in SM [29]). Then, we plug the inferred parameter values

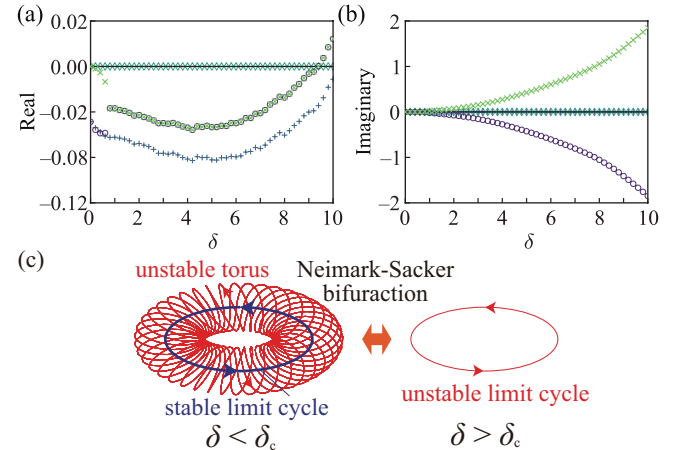


FIG. 3. Stability analysis of the anti-phase synchronized periodic solution, based on the Stuart-Landau oscillator system estimated from time series data of a fluid system. Here, we neglect the non-resonant terms $I^{(0)}$, $I^{(2)}\bar{z}_k$, and $I^{(4)}\bar{z}_\ell$ in Eq. (7). (a) Real part of the Floquet exponents. (b) Imaginary part of the Floquet exponents. (c) Schematic illustration that shows the bifurcation structure. The stable limit cycle collides with an unstable torus and destabilizes at $\delta = \delta_c \simeq 9.0$.

into the obtained eigenvalues ($\lambda_{\text{amp}}^{(\text{anti})}$ in Eq. (S55)) of the fixed point corresponding to the anti-phase synchrony. The eigenvalues are shown in Figs. S3(a) and S3(b). We observe that the real parts of a pair of exponents become positive at $\delta \simeq \delta_c$ while their imaginary parts are non-vanishing. This implies a Neimark-Sacker bifurcation. This is likely to be a subcritical one because we do not observe quasi-periodic dynamics for $\delta > \delta_c$; an unstable torus should exist for $\delta < \delta_c$ as schematically shown in Fig. S3(c).

By the linear stability analysis under the neglection of non-resonant terms, the qualitative characteristics for the Neimark-Sacker bifurcation can be reproduced; however the bifurcation point differs quantitatively if compared to the numerical simulation results shown in Fig. 1(e). The numerical linear stability analysis including non-resonant terms can improve the reproduction of the numerical simulation results as shown in Sect. VI of SM [29].

We developed and validated a method to estimate the coupled Stuart-Landau equation from the waveforms of two coupled oscillators. This approach was tested on systems modeled by the VDP equation and fluid dynamics. Its strength lies in fitting a universal equation near a supercritical Hopf bifurcation, rather than relying on detailed system-specific models. This allows for minimal parameters and fitting using short time series, which are expected to reduce overfitting risk. The method captures essential amplitude dynamics, which phase models cannot, and successfully uncovers that the anti-phase state disappears via a Neimark-Sacker bifurcation in the coupled fluid system.

Another key feature and a major advantage of this estimation method lie in its flexibility in time series selec-

tion: any two independent observables can be utilized. This is possible because the transformation to the variables of the Stuart-Landau equation is itself estimated, allowing the method to adapt to a wide range of data sources. This adaptability significantly broadens its applicability across diverse systems. While this study used two observables, future work will explore estimation from a single observable, possibly using time delays or Hilbert transforms.

As shown in Sect. VII and Fig. S4 in SM [29], even a single time series can yield accurate estimates in coupled VDP oscillators. Notably, solely from a time series that converges in-phase synchrony, our method can predict the existence of the stable anti-phase state and the basin structure. However, in fluid systems, results may depend on the time series used, indicating the need for further refinement, such as improving the cost function.

As an alternative approach to our normal-form-based inference, Koopman-based methods provide a general operator-theoretic representation of nonlinear dynamics and have proven useful for prediction and modal decomposition in complex systems [31, 32]. In principle, Koopman eigenfunctions can also provide meaningful phase-amplitude coordinates through connections to isochrons and isostables [33, 34]. Recent work has even reconstructed phase-amplitude network models directly from observed signals using Koopman-eigenfunction-based parameterizations [35]. Our strategy targets a different

regime and objective. By focusing on oscillators near a supercritical Hopf bifurcation, we leverage the universality of the Stuart-Landau normal form and infer a phase-amplitude model with a small number of parameters. This compact, equation-based representation facilitates mechanistic interpretation and makes subsequent bifurcation and stability analysis straightforward, which is essential for characterizing synchronization transitions in our applications.

ACKNOWLEDGMENTS

We thank István Z. Kiss and John L. Hudson for motivating discussions. This work was supported by JST SPRING Grant Number JPMJSP2109 (Y. Araya), by the Cooperative Research Program of “Network Joint Research Center for Materials and Devices” (Nos. 20245003 (Y. Araya) and 20244003 (H. Kitahata)), and by JSPS KAKENHI Grants Nos. JP21K13891 and JP24K06972 (H. Ito); JP21K12056 and JP25K15258 (H. Kori); JP24K06978, JP24K22311, and JP25K00918 (H. Kitahata). This work was also supported by JSPS Core-to-Core Program “Advanced core-to-core network for the physics of self-organizing active matter (JPJSCCA20230002)” and MEXT Promotion of Distinctive Joint Usage/Research Center Support Program (JP-MXP0724020292).

- [1] A. T. Winfree, *The geometry of biological time* (Springer-Verlag, 2001).
- [2] Y. Kuramoto, *Chemical Oscillations, Waves, and Turbulence* (Springer-Verlag, 1984).
- [3] A. Pikovsky, M. Rosenblum, and J. Kurths, *Synchronization: A universal concept in nonlinear sciences* (Cambridge University Press, 2001).
- [4] P. Ashwin, S. Coombes, and R. Nicks, Mathematical frameworks for oscillatory network dynamics in neuroscience, *J. Math. Neurosci.* **6**, 1 (2016).
- [5] E. A. Martens, S. Thutupalli, A. Fourriere, and O. Hallelschek, Chimera states in mechanical oscillator networks, *Proc. Natl. Acad. Sci. USA* **110**, 10563 (2013).
- [6] G. H. Goldsztein, A. N. Nadeau, and S. H. Strogatz, Synchronization of clocks and metronomes: A perturbation analysis based on multiple timescales, *Chaos* **31**, 023109 (2021).
- [7] Y. Kato and H. Kori, Weakly nonlinear analysis on synchronization and oscillation quenching of coupled mechanical oscillators, *Sci. Rep.* **14**, 1461 (2024).
- [8] I. Z. Kiss, Y. Zhai, and J. L. Hudson, Emerging coherence in a population of chemical oscillators, *Science* **296**, 1676 (2002).
- [9] I. Z. Kiss, C. G. Rusin, H. Kori, and J. L. Hudson, Engineering complex dynamical structures: Sequential patterns and desynchronization, *Science* **316**, 1886 (2007).
- [10] M. Toiya, H. O. González-Ochoa, V. K. Vanag, S. Fraden, and I. R. Epstein, Synchronization of chemical micro-oscillators, *J. Phys. Chem. Lett.* **1**, 1241 (2010).
- [11] L. Glass, Synchronization and rhythmic processes in physiology, *Nature* **410**, 277 (2001).
- [12] J. R. Clay and R. L. DeHaan, Fluctuations in interbeat interval in rhythmic heart-cell clusters. role of membrane voltage noise, *Biophys. J.* **28**, 377 (1979).
- [13] S. Yamaguchi, H. Isejima, T. Matsuo, R. Okura, K. Yagita, M. Kobayashi, and H. Okamura, Synchronization of cellular clocks in the suprachiasmatic nucleus, *Science* **302**, 1408 (2003).
- [14] N. Uchida and R. Golestanian, Synchronization and collective dynamics in a carpet of microfluidic rotors, *Phys. Rev. Lett.* **104**, 178103 (2010).
- [15] R. Golestanian, J. M. Yeomans, and N. Uchida, Hydrodynamic synchronization at low reynolds number, *Soft Matter* **7**, 3074 (2011).
- [16] D. R. Brumley, K. Y. Wan, M. Polin, and R. E. Goldstein, Flagellar synchronization through direct hydrodynamic interactions, *elife* **3**, e02750 (2014).
- [17] H. Nakao, Phase reduction approach to synchronization of nonlinear oscillators, *Contemporary Physics* **57**, 188 (2016).
- [18] H. Kori, C. G. Rusin, I. Z. Kiss, and J. L. Hudson, Synchronization engineering: Theoretical framework and application to dynamical clustering, *Chaos* **18**, 026111 (2008).
- [19] I. T. Tokuda, S. Jain, I. Z. Kiss, and J. L. Hudson, Inferring phase equations from multivariate time series, *Phys. Rev. Lett.* **99**, 064101 (2007).
- [20] K. A. Blaha, A. Pikovsky, M. Rosenblum, M. T. Clark,

C. G. Rusin, and J. L. Hudson, Reconstruction of two-dimensional phase dynamics from experiments on coupled oscillators, *Phys. Rev. E* **84**, 046201 (2011).

[21] T. Arai, Y. Kawamura, and T. Aoyagi, Extracting phase coupling functions between collectively oscillating networks from time-series data, *J. Phys. Soc. Jpn.* **91**, 124001 (2022).

[22] M. Rosenblum and A. Pikovsky, Inferring connectivity of an oscillatory network via the phase dynamics reconstruction, *Front. Netw. Physiol.* **3**, 1298228 (2023).

[23] A. Matsuki, H. Kori, and R. Kobayashi, Network inference applicable to both synchronous and desynchronous systems from oscillatory signals, *PLOS Complex Systems* **2**, e0000063 (2025).

[24] Y. A. Kuznetsov, *Elements of Applied Bifurcation Theory*, 3rd ed., Applied Mathematical Sciences, Vol. 112 (Springer, 2004).

[25] E. Gengel, E. Teichmann, M. Rosenblum, and A. Pikovsky, High-order phase reduction for coupled oscillators, *J. Phys.: Complex.* **2**, 015005 (2021).

[26] D. Wilson and B. Ermentrout, Phase Models beyond Weak Coupling, *Phys. Rev. Lett.* **123**, 164101 (2019).

[27] J. Guckenheimer and P. Holmes, *Nonlinear Oscillations, Dynamical Systems, and Bifurcations of Vector Fields* (Springer-Verlag, 1983).

[28] S. Wiggins, *Introduction to Applied Nonlinear Dynamical Systems and Chaos* (Springer, 2003).

[29] See supplemental material for the detailed calculation and related figures.

[30] Y. Araya, H. Ito, and H. Kitahata, Two-dimensional hydrodynamic simulation for synchronized oscillatory flows in two collapsible channels connected in parallel, *Phys. Rev. E* **109**, 054201 (2024).

[31] M. O. Williams, I. G. Kevrekidis, and C. W. Rowley, A data-driven approximation of the Koopman operator: Extending dynamic mode decomposition, *Journal of Nonlinear Science* **25**, 1307 (2015).

[32] I. Mezić, Analysis of fluid flows via spectral properties of the Koopman operator, *Annual Review of Fluid Mechanics* **45**, 357 (2013).

[33] A. Mauroy, I. Mezić, and J. Moehlis, Isostables, isochrons, and Koopman spectrum for the action-angle representation of stable fixed point dynamics, *Physica D: Nonlinear Phenomena* **261**, 19 (2013).

[34] A. Mauroy and I. Mezić, Global computation of phase-amplitude reduction for limit-cycle dynamics, *Chaos: An Interdisciplinary Journal of Nonlinear Science* **28**, 073108 (2018).

[35] A. Yeldesbay, G. Huguet, and S. Daun, Reconstruction of phase-amplitude dynamics from signals of a network of oscillators, *Chaos: An Interdisciplinary Journal of Nonlinear Science* **35**, 043140 (2025).

SUPPLEMENTAL MATERIAL

I. EXPRESSIONS FOR THE PARAMETERS RELATED TO VARIABLE TRANSFORMATIONS

We express two observables ϕ and ψ of the single oscillation in terms of the complex amplitude z , which follows the Stuart-Landau equation. Two observables should generally be expanded with respect to z and \bar{z} as

$$\phi = \sum_{n,m \geq 0}^{n+m=3} \Phi^{(n,m)} z^n \bar{z}^m + \mathcal{O}(4), \quad (\text{S1})$$

$$\psi = \sum_{n,m \geq 0}^{n+m=3} \Psi^{(n,m)} z^n \bar{z}^m + \mathcal{O}(4), \quad (\text{S2})$$

where $\Phi^{(n,m)}$ and $\Psi^{(n,m)}$ are complex constants, and n and m are integers greater than or equal to 0. Note that $\Phi^{(n,m)} = \bar{\Phi}^{(m,n)}$ and $\Psi^{(n,m)} = \bar{\Psi}^{(m,n)}$ because ϕ and ψ are real. From Eqs. (S1) and (S2), we obtain the transformation:

$$w = z + h_2(z, \bar{z}) + h_3(z, \bar{z}) + \mathcal{O}(4), \quad (\text{S3})$$

where

$$w = q_\phi \phi + q_\psi \psi - C^{(0,0)}, \quad (\text{S4})$$

$$h_2(z, \bar{z}) = C^{(2,0)} z^2 + C^{(1,1)} z \bar{z} + C^{(0,2)} \bar{z}^2, \quad (\text{S5})$$

$$h_3(z, \bar{z}) = C^{(3,0)} z^3 + C^{(2,1)} z^2 \bar{z} + C^{(1,2)} z \bar{z}^2 + C^{(0,3)} \bar{z}^3, \quad (\text{S6})$$

$$C^{(n,m)} = q_\phi \Phi^{(n,m)} + q_\psi \Psi^{(n,m)}, \quad (\text{S7})$$

$$q_\phi = \frac{\Psi^{(0,1)}}{\Phi^{(1,0)} \Psi^{(0,1)} - \Phi^{(0,1)} \Psi^{(1,0)}}, \quad (\text{S8})$$

$$q_\psi = \frac{-\Phi^{(0,1)}}{\Phi^{(1,0)} \Psi^{(0,1)} - \Phi^{(0,1)} \Psi^{(1,0)}}. \quad (\text{S9})$$

In the same way as the calculation of the normal form for the Hopf bifurcation with the near-identity transformation, $\Phi^{(n,m)}$ and $\Psi^{(n,m)}$ should be determined so that z follows the Stuart-Landau equation. Note that we choose $C^{(2,1)}$ to be zero because it has an arbitrary value. Inverse near-identity transformation is expressed as

$$z = w - h_2 - h_3 + h_2 \frac{\partial h_2}{\partial z} + \bar{h}_2 \frac{\partial h_2}{\partial \bar{z}} + \mathcal{O}(4), \quad (\text{S10})$$

where the omitted arguments of h_2 , h_3 , $\partial h_2/\partial z$, and $\partial h_2/\partial \bar{z}$ at the righthand side are w and \bar{w} . Therefore, we have to infer q_ϕ , q_ψ , $C^{(0,0)}$, $C^{(2,0)}$, $C^{(1,1)}$, $C^{(0,2)}$, $C^{(3,0)}$, $C^{(1,2)}$, $C^{(0,3)}$ to obtain the complex amplitude from the time series of two observables.

To decrease the number of inferred parameters, we adopt the Fourier coefficients of the two observables ϕ and ψ . First, we measure the oscillation period by measuring the time interval between peaks of the time series of ϕ and ψ after the transient process and determine $b - d$. Then, we expand the time series into the Fourier series as

$$\phi = \sum_n \phi_n \exp(in(b - d)t) \quad (\text{S11})$$

and

$$\psi = \sum_n \psi_n \exp(in(b - d)t). \quad (\text{S12})$$

We substitute the explicit forms of ϕ and ψ and the stable limit cycle solution

$$z = \exp(i(b - d)t) \quad (\text{S13})$$

into Eqs. (S1) and (S2). From the obtained equation, the relation for each wave number gives

$$\phi_0 = \Phi^{(0,0)} + \Phi^{(1,1)}, \quad (\text{S14})$$

$$\psi_0 = \Psi^{(0,0)} + \Psi^{(1,1)}, \quad (\text{S15})$$

$$\phi_1 = \Phi^{(1,0)} + \Phi^{(2,1)}, \quad (\text{S16})$$

$$\psi_1 = \Psi^{(1,0)} + \Psi^{(2,1)}, \quad (\text{S17})$$

$$\phi_2 = \Phi^{(2,0)}, \quad (\text{S18})$$

$$\psi_2 = \Psi^{(2,0)}, \quad (\text{S19})$$

$$\phi_3 = \Phi^{(3,0)}, \quad (\text{S20})$$

$$\psi_3 = \Psi^{(3,0)}. \quad (\text{S21})$$

Because $C^{(2,1)}$ is equal to zero, $\Phi^{(n,m)}$ and $\Psi^{(n,m)}$ follow

$$\Psi^{(0,1)}\Phi^{(2,1)} - \Phi^{(0,1)}\Psi^{(2,1)} = 0. \quad (\text{S22})$$

Therefore, $\Phi^{(2,1)}$ and $\Psi^{(2,1)}$ can be expressed as $\Phi^{(2,1)} = \bar{C}^{(1,2)}\Phi^{(0,1)}$, $\Psi^{(2,1)} = \bar{C}^{(1,2)}\Psi^{(0,1)}$. In summary, the parameters are expressed using the Fourier coefficients as

$$q_\phi = (\psi_{-1} - C^{(1,2)}\psi_1)/(\phi_1\psi_{-1} - \psi_1\phi_{-1}), \quad (\text{S23})$$

$$q_\psi = -(\phi_{-1} - C^{(1,2)}\phi_1)/(\phi_1\psi_{-1} - \psi_1\phi_{-1}), \quad (\text{S24})$$

$$C^{(0,0)} = q_\phi\phi_0 + q_\psi\psi_0 - C^{(1,1)}, \quad (\text{S25})$$

$$C^{(2,0)} = q_\phi\phi_2 + q_\psi\psi_2, \quad (\text{S26})$$

$$C^{(0,2)} = q_\phi\phi_{-2} + q_\psi\psi_{-2}, \quad (\text{S27})$$

$$C^{(3,0)} = q_\phi\phi_3 + q_\psi\psi_3, \quad (\text{S28})$$

$$C^{(0,3)} = q_\phi\phi_{-3} + q_\psi\psi_{-3}. \quad (\text{S29})$$

II. STABILITY ANALYSIS FOR COUPLED VAN DER POL OSCILLATORS

We analytically derive the Stuart-Landau equation from the van der Pol (VDP) equation using a near-identity transformation. By introducing $v \equiv \dot{x}$, the VDP equation is rewritten as a two-dimensional dynamical system,

$$\dot{x} = v, \quad (\text{S30})$$

$$\dot{v} = (\mu - x^2)v - x. \quad (\text{S31})$$

One of the eigenvalues λ at the fixed point $(x, v) = (0, 0)$ is obtained as

$$\lambda = \frac{\mu}{2} + i\sqrt{1 - \frac{\mu^2}{4}} \quad (\text{S32})$$

by the linear stability analysis. Since we consider the onset of the Hopf bifurcation point, we assume $1 - \mu^2/4 > 0$. A right eigenvector $\mathbf{p} = {}^t(p_x, p_v)$ corresponding to λ satisfies $p_v = \lambda p_x$. Defining the left eigenvector $\mathbf{q} = (q_x, q_v)$ so that

$$p_x q_x + p_v q_v = 1 \quad (\text{S33})$$

and

$$\bar{p}_x q_x + \bar{p}_v q_v = 0, \quad (\text{S34})$$

we obtain

$$(q_x, q_v) = \frac{\bar{p}_x}{|p_x|^2(\bar{\lambda} - \lambda)}(\bar{\lambda}, -1). \quad (\text{S35})$$

It should be noted that the x -component of the right eigenvector p_x can be arbitrarily chosen. Considering that p_x is a complex number, the absolute value of p_x determines the ratio of $|\mathbf{p}|$ and $|\mathbf{q}|$, and the argument of p_x determines the correspondence of the phase origins of the VDP equation and the Stuart-Landau equation.

We define the complex amplitude z by $z \equiv q_x x + q_v v$ using the right eigenvector. Then, x and v are expressed as $x = zp_x + \bar{z}\bar{p}_x$, and $v = zp_v + \bar{z}\bar{p}_v$. The time-evolution equation for z is thus

$$\dot{z} = \lambda z - \lambda q_v p_x^3 z^3 - q_v p_x^2 \bar{p}_x (\bar{\lambda} + 2\lambda) z^2 \bar{z} - q_v p_x \bar{p}_x^2 (2\bar{\lambda} + \lambda) z \bar{z}^2 - \bar{\lambda} q_v \bar{p}_x^3 \bar{z}^3. \quad (\text{S36})$$

Applying the near-identity transformation

$$z \mapsto z + C^{(3,0)} z^3 + C^{(1,2)} z \bar{z}^2 + C^{(0,3)} \bar{z}^3, \quad (\text{S37})$$

we obtain

$$C^{(3,0)} = \frac{i\mu}{4\sqrt{1-\mu^2/4}} \frac{p_x^2}{|p_x|^2}, \quad (\text{S38})$$

$$C^{(1,2)} = \left(-\frac{\mu^2}{4} + i \frac{\mu + \mu^3/2}{4\sqrt{1-\mu^2/4}} \right) \frac{\bar{p}_x^2}{|p_x|^2}, \quad (\text{S39})$$

$$C^{(0,3)} = \left(-\frac{\mu^2}{32-6\mu^2} + i \frac{\mu - \mu^3/8}{(8-3\mu^2/2)\sqrt{1-\mu^2/4}} \right) \frac{\bar{p}_x^4}{|p_x|^4}. \quad (\text{S40})$$

Under this transformation, time evolution of z is given as

$$\dot{z} = \left(\frac{\mu}{2} + i\sqrt{1-\frac{\mu^2}{4}} \right) z - \left(\frac{1}{2} - i\frac{3\mu}{4\sqrt{1-\mu^2/4}} \right) |p_x|^2 z^2 \bar{z} + \mathcal{O}(5). \quad (\text{S41})$$

Choosing $|p_x|^2 = \mu$ so that the modulus of the complex amplitude is 1 on the limit cycle solution, we get

$$\dot{z} = \left(\frac{\mu}{2} + i \right) z - \left(\frac{\mu}{2} - i \frac{3\mu^2}{4\sqrt{1-\mu^2/4}} \right) z^2 \bar{z} + \mathcal{O}(5). \quad (\text{S42})$$

The transformation between z and (x, v) has still one free parameter that reflects the phase relationship. If we set it so that $\arg z = 0$ at $v = 0$ with $x > 0$, then the explicit transformation is given by setting $p_x = \sqrt{\mu(1-\mu^2/4)} + i\mu\sqrt{\mu}/2$. In this case, the linear transformation is given as

$$z = \frac{x - (\mu/2)v}{2\sqrt{\mu(1-\mu^2/4)}} - i\frac{v}{2\sqrt{\mu}}, \quad (\text{S43})$$

and

$$(x, v) = \left(\sqrt{\mu(4-\mu^2)} \operatorname{Re} z - \mu\sqrt{\mu} \operatorname{Im} z, -2\sqrt{\mu} \operatorname{Im} z \right). \quad (\text{S44})$$

The coefficients for the near-identity transformation are also explicitly given as

$$C^{(3,0)} = -\frac{\mu^2}{4} + i \frac{\mu(2-\mu^2)}{4\sqrt{4-\mu^2}}, \quad (\text{S45})$$

$$C^{(1,2)} = \frac{\mu^4}{4} + i \frac{2+2\mu^2-\mu^4}{4\sqrt{4-\mu^2}}, \quad (\text{S46})$$

$$C^{(0,3)} = \frac{\mu^2(7-3\mu^2)}{32-6\mu^2} + i \frac{\mu(8-13\mu^2+3\mu^4)}{2(16-3\mu^2)\sqrt{4-\mu^2}}. \quad (\text{S47})$$

Considering that our inference method uses the third-order near-identity transformation, μ is a small parameter and the analysis is precise upto the order of μ^1 . Thus, for the comparison to the inference results, we adopt $a = \mu/2$, $b = 1$, and $d = 0$ by neglecting the terms of $\mathcal{O}(\mu^2)$.

Next, we transform the coupled VDP equations with setting $\dot{x}_1 = v_1$, $\dot{x}_2 = v_2$. Applying the near-identity transformation defined by the single oscillator, (x_1, v_1) and (x_2, v_2) are mapped to complex amplitudes z_1 and z_2 , respectively, yielding

$$\dot{z}_1 = \left(\frac{\mu}{2} + i \right) z_1 - \frac{\mu}{2} z_1^2 \bar{z}_1 + I(z_1, z_2) + \mathcal{O}(\mu^2), \quad (\text{S48})$$

$$\dot{z}_2 = \left(\frac{\mu}{2} + i \right) z_2 - \frac{\mu}{2} z_2^2 \bar{z}_2 + I(z_2, z_1) + \mathcal{O}(\mu^2), \quad (\text{S49})$$

where the linear part of the interaction term I is

$$I(z_1, z_2) = \left(\frac{I_v}{2} - i \frac{2I_x + \mu I_v}{4} \right) (z_2 - z_1) - \left(\frac{I_v}{2} + i \frac{2I_x + \mu I_v}{4} \right) \frac{\bar{p}_x^2}{|p_x|^2} (\bar{z}_2 - \bar{z}_1). \quad (\text{S50})$$

Thus, $I^{(0)} = 0$, $I^{(1)} = -I_v/2 + i(2I_x + \mu I_v)/4$, and $I^{(3)} = I_v/2 - i(2I_x + \mu I_v)/4$. The coefficients $I^{(2)}$ and $I^{(4)}$ for the complex conjugates \bar{z}_1 and \bar{z}_2 depend on p_x , but they have relation $I^{(2)} = -I^{(4)}$ and $|I^{(1)}| = |I^{(2)}| = |I^{(3)}| = |I^{(4)}|$ independent of the choice of p_x . In the case of the transformation in Eqs. (S43) and (S44), we obtain

$$I^{(2)} = -I^{(4)} = (\mu I_x + I_v)/2 + i(2I_x - \mu I_v)/4.$$

III. DETAILED CALCULATION FOR THE LINEAR STABILITY ANALYSES OF COUPLED STUART-LANDAU EQUATIONS

Here, we analyze the stability of the coupled Stuart-Landau equation (Eq. (7) in the main text) under the assumption that the non-resonance terms $I^{(0)}$, $I^{(2)}\bar{z}_1$ and $I^{(4)}\bar{z}_2$ are neglected. It should be noted that the limit cycles corresponding to the in-phase and anti-phase states in the phase space of (z_1, z_2) correspond to fixed points in the (r_+, r_-, θ_-) space. First, we obtain the forms with polar coordinates $z_1 = r_1 e^{i\theta_1}$ and $z_2 = r_2 e^{i\theta_2}$ expressed as

$$\dot{r}_+ = a(r_+ - r_+^3 - 3r_+ r_-^2) + \text{Re } I^{(1)} r_+ + \text{Re } I^{(3)} r_+ \cos \theta_- - \text{Im } I^{(3)} r_- \sin \theta_-, \quad (\text{S51})$$

$$\dot{r}_- = a(r_- - 3r_+^2 r_- - r_-^3) + \text{Re } I^{(1)} r_- - \text{Re } I^{(3)} r_- \cos \theta_- + \text{Im } I^{(3)} r_+ \sin \theta_-, \quad (\text{S52})$$

$$\dot{\theta}_- = -4dr_+ r_- - \text{Re } I^{(3)} \frac{2r_+^2 + 2r_-^2}{r_+^2 - r_-^2} \sin \theta_- - \text{Im } I^{(3)} \frac{4r_+ r_-}{r_+^2 - r_-^2} \cos \theta_-, \quad (\text{S53})$$

where $r_\pm = (r_1 \pm r_2)/2$ and $\theta_- = \theta_1 - \theta_2$. We apply the linear stability analysis to the limit cycle, where $\dot{r}_+ = 0$, $\dot{r}_- = 0$, and $\dot{\theta}_- = 0$. The solution corresponding to the in-phase synchronization is given as $(r_+^*, r_-^*, \theta_-^*) = (\sqrt{1 + (\text{Re } I^{(1)} + \text{Re } I^{(3)})/a}, 0, 0)$, and that corresponding to the anti-phase synchronization is given as $(r_+^*, r_-^*, \theta_-^*) = (\sqrt{1 + (\text{Re } I^{(1)} - \text{Re } I^{(3)})/a}, 0, \pi)$. The eigenvalues of the Jacobi matrix for the linearized equations are obtained as

$$\begin{aligned} \lambda_{\text{amp}}^{(\text{in})} = & -2 \left(a + \text{Re } I^{(1)} + \text{Re } I^{(3)} \right), \\ & - a - \text{Re } I^{(1)} - 3\text{Re } I^{(3)} \pm \sqrt{\left(a + \text{Re } I^{(1)} + \text{Re } I^{(3)} \right)^2 - 4\text{Im } I^{(3)} \left\{ \text{Im } I^{(3)} + d \left(1 + \frac{\text{Re } I^{(1)} + \text{Re } I^{(3)}}{a} \right) \right\}} \end{aligned} \quad (\text{S54})$$

for the in-phase synchronization, and

$$\begin{aligned} \lambda_{\text{amp}}^{(\text{anti})} = & -2 \left(a + \text{Re } I^{(1)} - \text{Re } I^{(3)} \right), \\ & - a - \text{Re } I^{(1)} + 3\text{Re } I^{(3)} \pm \sqrt{\left(a + \text{Re } I^{(1)} - \text{Re } I^{(3)} \right)^2 - 4\text{Im } I^{(3)} \left\{ \text{Im } I^{(3)} - d \left(1 + \frac{\text{Re } I^{(1)} - \text{Re } I^{(3)}}{a} \right) \right\}} \end{aligned} \quad (\text{S55})$$

for the anti-phase synchronization. It should be noted that the Floquet exponents for the original system are given by these eigenvalues and 0, where 0 corresponds to the neutral mode in the direction of the trajectory.

From the results shown in Section II of SM, the parameters a , c , d , $I^{(1)}$, and $I^{(3)}$ are given for the coupled VDP equation. Under the assumption that the non-resonant terms $I^{(0)}$, $I^{(2)}z$, $I^{(4)}\bar{z}$ in the coupling terms, are neglected, the eigenvalues for the in-phase and anti-phase synchronizations are expressed as

$$\lambda_{\text{amp}}^{(\text{in})} = -\mu, -\frac{\mu}{2} - I_v \pm \sqrt{\left(\frac{\mu}{2}\right)^2 - \left(I_x + \frac{\mu I_v}{2}\right)^2}, \quad (\text{S56})$$

and

$$\lambda_{\text{amp}}^{(\text{anti})} = -\mu + 2I_v, -\frac{\mu}{2} + 2I_v \pm \sqrt{\left(\frac{\mu}{2} - I_v\right)^2 - \left(I_x + \frac{\mu I_v}{2}\right)^2}, \quad (\text{S57})$$

respectively. For the parameter region $\mu > 0$, $I_x > 0$, and $I_v > 0$, which corresponds to the region shown in Fig. 4 in the main text, all of the real parts of the eigenvalues for the in-phase synchronization are always negative, indicating that the in-phase synchronization is stable. In contrast, the anti-phase synchronization mode becomes unstable via a Neimark-Sacker bifurcation at

$$I_v = \frac{\mu}{4}, \quad (\text{S58})$$

and a pitchfork bifurcation at

$$\left(I_x + \frac{\mu I_v}{2}\right)^2 + 3\left(I_v - \frac{\mu}{6}\right)^2 = \frac{\mu^2}{12}. \quad (\text{S59})$$

Next, we consider the adiabatic approximation with respect to the amplitudes. We assume $\dot{r}_{\pm} = 0$ and obtain a time evolution equation for θ_- , which is valid close to the fixed points corresponding to the in-phase and anti-phase states ($\theta_- = 0$ and π , respectively). The linearized equation around the fixed point $\theta_- = 0$ is given as

$$\delta\dot{\theta}_- = \left[-4dr_{+0}K_0 - 4\text{Im}I^{(3)}\frac{K_0}{r_{+0}} - 2\text{Re}I^{(3)} \right] \delta\theta_-, \quad (\text{S60})$$

where r_{+0} is the steady-state solution $r_{+0} = \sqrt{1 + (\text{Re}I^{(1)} + \text{Re}I^{(3)})/a}$ and K_0 is given as

$$K_0 = \frac{r_{+0}\text{Im}I^{(3)}}{2(a + \text{Re}I^{(1)} + 2\text{Re}I^{(3)})}. \quad (\text{S61})$$

Thus, the eigenvalue for the linearized equation is given as

$$\lambda_{\text{ad}}^{(\text{in})} = -\frac{2\text{Im}I^{(3)}(ad + d\text{Re}I^{(1)} + d\text{Re}I^{(3)} + a\text{Im}I^{(3)})}{a(a + \text{Re}I^{(1)} + 2\text{Re}I^{(3)})} - 2\text{Re}I^{(3)} \quad (\text{S62})$$

The linearized equation around the fixed point $\theta_- = \pi$, i.e., anti-phase synchronization, is also given in the same manner as

$$\delta\dot{\theta}_- = \left[-4dr_{+\pi}K_{\pi} + 4\text{Im}I^{(3)}\frac{K_{\pi}}{r_{+\pi}} + 2\text{Re}I^{(3)} \right] \delta\theta_-, \quad (\text{S63})$$

where $r_{+\pi}$ is the steady-state solution $r_{+\pi} = \sqrt{1 + (\text{Re}I^{(1)} - \text{Re}I^{(3)})/a}$ and K_{π} is given as

$$K_{\pi} = -\frac{r_{+\pi}\text{Im}I^{(3)}}{2(a + \text{Re}I^{(1)} - 2\text{Re}I^{(3)})}. \quad (\text{S64})$$

Thus, the eigenvalue for the linearized equation is given as

$$\lambda_{\text{ad}}^{(\text{anti})} = \frac{2\text{Im}I^{(3)}(ad + d\text{Re}I^{(1)} - d\text{Re}I^{(3)} - a\text{Im}I^{(3)})}{a(a + \text{Re}I^{(1)} - 2\text{Re}I^{(3)})} + 2\text{Re}I^{(3)}. \quad (\text{S65})$$

For the coupled VDP equations, the eigenvalues for the in-phase and anti-phase states are calculated as

$$\lambda_{\text{ad}}^{(\text{in})} = -I_v - \frac{(2I_x + \mu I_v)^2}{4(\mu + I_v)}, \quad (\text{S66})$$

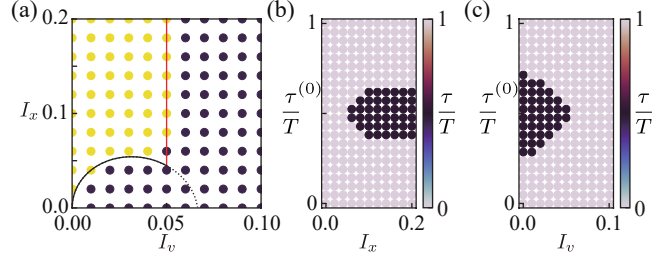


FIG. S1. Numerical results for the coupled van der Pol (VDP) equations. (a) Phase diagram for the anti-phase synchrony, where the yellow and purple circles indicate stable and unstable anti-phase states, respectively. From the analysis using the coupled Stuart-Landau equations with non-resonance terms neglected, the anti-phase synchrony is stable when all the real values of $\lambda_{\text{amp}}^{(\text{anti})}$ in Eq. (S57) are negative. The stability boundary is shown by the black line (Eq. (S59)) and red solid line (Eq. (S58)). In contrast, using the equation with the adiabatic approximation, the stability boundary is given by $\lambda_{\text{ad}}^{(\text{anti})} = 0$; i.e. Eq. (S59), which is represented by the combination of the black solid and dashed lines. (b, c) Normalized phase difference τ/T in the final state depending on (ii) $\tau^{(0)}/T$ and I_x at $I_v = 0.03$ and (iii) $\tau^{(0)}/T$ and I_v at $I_x = 0.16$. $\tau^{(0)}/T$ is the initial normalized phase difference between two oscillators and T is the intrinsic period of the single oscillator.

and

$$\lambda_{\text{ad}}^{(\text{anti})} = I_v - \frac{(2I_x + \mu I_v)^2}{4(\mu - 3I_v)}, \quad (\text{S67})$$

respectively. Thus, for $\mu > 0$, $I_x > 0$, and $I_v > 0$, the in-phase synchronization is always stable, while the anti-phase synchronization becomes unstable at the condition given by Eq. (S59) via a pitchfork bifurcation.

Finally, we consider the case using the coupled phase equations. From a single Stuart-Landau equation, we obtain the phase equation as

$$\dot{\theta} = b - d, \quad (\text{S68})$$

since the stable amplitude is 1. Then, we obtain the coupled equation as

$$\dot{\theta}_k = b - d + \text{Im}I^{(1)} + \text{Re}I^{(3)} \sin(\theta_\ell - \theta_k) + \text{Im}^{(3)} \cos(\theta_\ell - \theta_k). \quad (\text{S69})$$

By setting $\theta_- = \theta_1 - \theta_2$, we obtain

$$\dot{\theta}_- = -2\text{Re}I^{(3)} \sin \theta_-. \quad (\text{S70})$$

The eigenvalues for in-phase and anti-phase synchronizations are given as

$$\lambda_{\text{phase}}^{(\text{in})} = -2\text{Re}I^{(3)}, \quad (\text{S71})$$

and

$$\lambda_{\text{phase}}^{(\text{anti})} = 2\text{Re}I^{(3)}, \quad (\text{S72})$$

respectively. For the coupled VDP equations, $\text{Re}I^{(3)} = I_v/2$, and therefore in-phase synchronization is stable and anti-phase synchronization is unstable for $\mu > 0$, $I_x > 0$, and $I_v > 0$. The analysis using the phase equation is only correct when the interaction is sufficiently weak; it cannot predict the stable anti-phase synchrony.

Figure S1 shows the stability boundaries of the anti-phase synchronization obtained from the eigenvalues without approximation and those with the adiabatic approximation. The former can anticipate both the Neimark-Sacker and pitchfork bifurcations, while the latter can anticipate only the pitchfork bifurcation. The boundary tangentially touches I_x -axis at the origin, which shows that the anti-phase synchronization is unstable for the small I_x and I_v .

The bifurcation line obtained from the linear stability analysis is quantitatively consistent with the numerical simulation results. We also show the bifurcation line obtained from the adiabatic approximation with respect to the amplitudes using black solid and dashed lines in Fig. S1(a). We can reproduce the pitchfork bifurcation line using the adiabatic approximation, while we fail to lead the Neimark-Sacker bifurcation line.

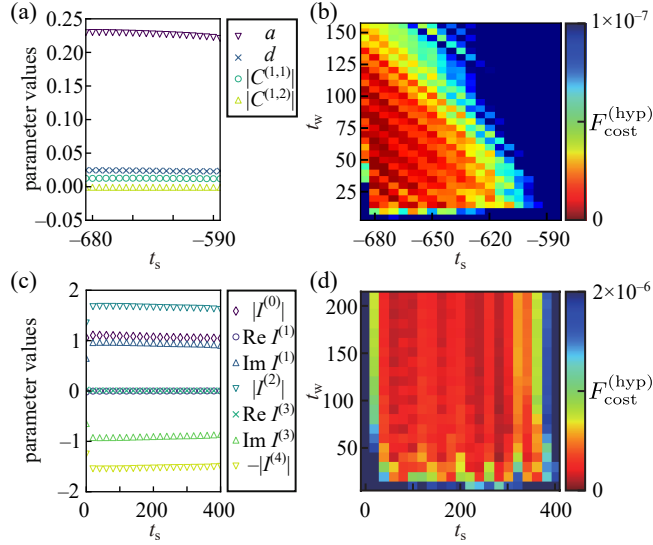


FIG. S2. t_s - and t_w -dependences of the inferred parameters in (a,b) the single system and (c,d) coupled system of the oscillatory flow obtained by numerical simulation. $t_w = 25$ for the panel (a) and $t_w = 100$ for the panel (c). $F_{\text{cost}}^{(3)}$ is the cost function to evaluate the robustness of parameters.

IV. NUMERICAL CALCULATION SETUPS FOR THE COUPLED VAN DER POL EQUATIONS

We performed the numerical calculation for $I_x = I_v = 0$ until $t = 0$ to ensure the convergence to each limit cycle, where we set the initial conditions $(x_1, \dot{x}_1) = (0.1, 0)$ at $t = -300$ and $(x_2, \dot{x}_2) = (0.1, 0)$ at $t = -300 + \tau^{(0)}$. $\tau^{(0)}$ is the initial time delay between the two oscillators. We changed the coupling strength from 0 to the appropriate values at $t = 0$ and continued the numerical calculations until $t = 300$. We set $\mu = 0.2$ and varied I_x and I_v in the range between $0 \leq I_v \leq 0.1$ and $0 \leq I_x \leq 0.2$. $\tau^{(0)}$ was varied from 0 to T in increments of $T/21$, where T is the intrinsic period of the single oscillator.

In the inference, we used the time series from $t = -T$ to 0 in increments of 0.01 to calculate the Fourier coefficients, those from $t = -300$ to -295 in increments of 0.1 to infer the single Stuart-Landau equation, and those from $t = 17.5$ to 35.5 in increments of 0.1 in the various initial conditions to infer the coupling terms. $t_s = -300, t_w = 5$ are employed in the single system and $t_s = 17.5, t_w = 18$ are employed in the coupled system.

V. NUMERICAL CALCULATION SETUPS FOR THE COUPLED COLLAPSIBLE CHANNELS

The details of the simulation method of the hydrodynamic flow in the coupled collapsible channels are described in the previous paper ([30] in the main text); the authors performed the hydrodynamic simulation of the coupled collapsible channels for the stretching stiffness $K_s = 1000$, which is not sufficiently close to the Hopf bifurcation point in the single oscillatory flow. Thus, we performed the hydrodynamic simulation again for $K_s = 1200$ with varying ϵ from 0 to 10 in increments of 0.2. We set the initial condition where the upper elastic wall is parallel to the x_1 -axis (see Fig. 1 in the main text) at $t = -700$ and the lower one is parallel to the x_1 -axis at $t = -700 + \tau^{(0)}$.

$\tau^{(0)}$ is the initial time delay between two oscillatory flows. We simulated for $\epsilon = 0$ until $t = 0$, changed ϵ to the appropriate values at $t = 0$, and continued the simulation until $t = 750$. $\tau^{(0)}$ was varied from 0 to T in increments of $T/34$, where T is a period at $\epsilon = 0$.

In the inference, we used the time series from $t = -T$ to $t = 0$ in increments of 0.0025 to calculate the Fourier coefficients, those from $t = -675$ to -625 in increments of 0.25 to infer the single Stuart-Landau equation; and those from 80 to 180 in increments of 0.25 in the various initial conditions to infer the coupling terms. These settings were appropriately selected based on the inference varying t_s and t_w shown in Figs. S2(b) and S2(d). Based on the results shown above, $t_s = -675, t_w = 50$ are employed in the single system and $t_s = 80, t_w = 100$ are employed in the coupled system in Fig. 3 in the main text.

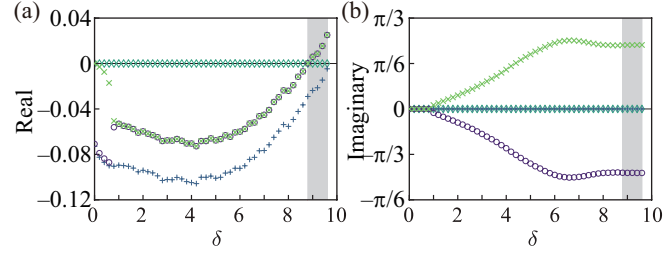


FIG. S3. Stability analysis of the anti-phase synchronized periodic solution, based on the Stuart-Landau oscillator system estimated from time series data of a fluid system. (a) Real part of the Floquet exponents. (b) Imaginary part of the Floquet exponents. The gray region represents the parameter range in which an unstable limit cycle exists; i.e., the left edge corresponds to $\delta = \delta_c$.

VI. NUMERICAL STABILITY ANALYSIS FOR THE COUPLED STUART-LANDAU EQUATIONS WITH NON-RESONANT TERMS

We also performed a numerical stability analysis of the solution corresponding to the anti-phase synchronization in the inferred coupled Stuart-Landau equations (S7) in the main text by numerically obtaining the solution and calculating the Floquet exponents. First, the solution (z_1^*, z_2^*) was represented by a Fourier series,

$$z_1^* = \sum_n c_n \exp(in\omega t), \quad (S73)$$

$$z_2^* = \sum_n c_n \exp(in\omega t + i\pi), \quad (S74)$$

and the Fourier coefficients c_n and the frequency ω were numerically obtained. It should be noted $c_{-1} = \bar{c}_1$. Substituting the Fourier expansion of the solution corresponding to the anti-phase synchronization into Eq. (7) in the main text, we obtain a nonlinear equation that determines ω and c_n :

$$\sum_{n=-N}^N i\omega c_n \exp(in\omega t) = G_1(z_1^*, z_2^*). \quad (S75)$$

To obtain the Fourier coefficients c_n and the frequency ω , we numerically minimized the cost function

$$F_{\text{cost}}^{(4)} = \int_0^{2\pi/\omega} \left(\sum_{n=-N}^N i\omega c_n \exp(in\omega t) - G_1(z_1^*, z_2^*) \right)^2 dt \quad (S76)$$

using the differential evolution method. Without loss of generality, we set $\text{Im } c_1 = 0$ to fix the arbitrary phase. Fourier modes with $-6 \leq n \leq 6$ were included in the numerical calculation. The time integral in the cost function $F_{\text{cost}}^{(4)}$ was evaluated with a resolution corresponding to 600 subdivisions of the period using the trapezoidal rule. Next, we measured the Floquet exponents by integrating the system over one period, starting from initial conditions given by the numerically obtained solution (z_1^*, z_2^*) with small perturbations. Numerical calculations were performed using four perturbed initial conditions: $(z_1^* + \varepsilon, z_2^*), (z_1^* + i\varepsilon, z_2^*), (z_1^*, z_2^* + \varepsilon), (z_1^*, z_2^* + i\varepsilon)$. The perturbation amplitude ε was chosen to be sufficiently small to probe the linear response while avoiding numerical inaccuracies.

In our calculation, we set $\varepsilon = 10^{-2}$. After one period, we obtained four sets of variables $(z_1^{(1)}, z_2^{(1)}), (z_1^{(2)}, z_2^{(2)}), (z_1^{(3)}, z_2^{(3)}), (z_1^{(4)}, z_2^{(4)})$, where the time evolution was calculated using the Euler method and the time step was set to $10^{-4} \times 2\pi/\omega$. Using the deviations from (z_1^*, z_2^*) , we evaluated the Floquet exponents λ_{AP} , which are the eigenvalues of the linear response matrix around the periodic solution, which is explicitly given by

$$\frac{1}{\varepsilon} \begin{pmatrix} \text{Re}(z_1^{(1)} - z_1^*) & \text{Re}(z_1^{(2)} - z_1^*) & \text{Re}(z_1^{(3)} - z_1^*) & \text{Re}(z_1^{(4)} - z_1^*) \\ \text{Im}(z_1^{(1)} - z_1^*) & \text{Im}(z_1^{(2)} - z_1^*) & \text{Im}(z_1^{(3)} - z_1^*) & \text{Im}(z_1^{(4)} - z_1^*) \\ \text{Re}(z_2^{(1)} - z_2^*) & \text{Re}(z_2^{(2)} - z_2^*) & \text{Re}(z_2^{(3)} - z_2^*) & \text{Re}(z_2^{(4)} - z_2^*) \\ \text{Im}(z_2^{(1)} - z_2^*) & \text{Im}(z_2^{(2)} - z_2^*) & \text{Im}(z_2^{(3)} - z_2^*) & \text{Im}(z_2^{(4)} - z_2^*) \end{pmatrix}. \quad (S77)$$

The numerically measured Floquet exponents λ_{AP} of the limit cycle corresponding to anti-phase synchronization are shown in Fig. S3. The real parts of the complex conjugate pair of λ_{AP} became positive at $\delta \simeq 8.2$, which indicated

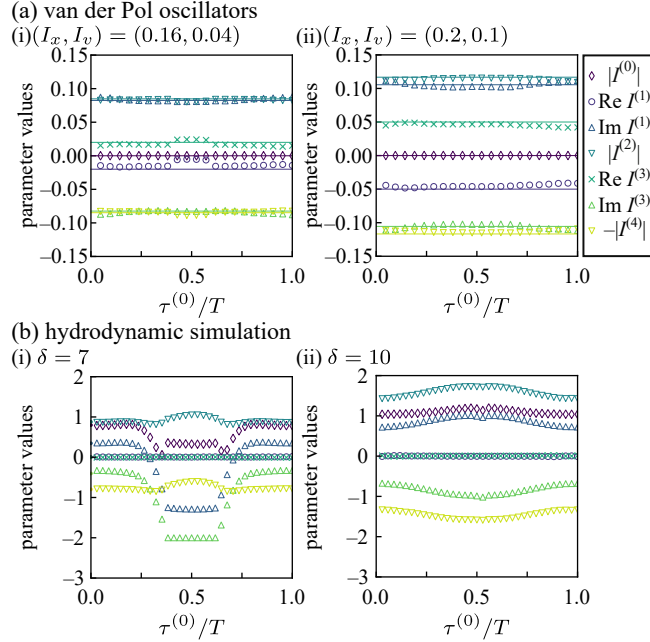


FIG. S4. Inferred parameters from the single time series of (a) VDP oscillators and (b) oscillatory flows in coupled collapsible channels. (i) In case that the in-phase and anti-phase states are bistable ($I_x = 0.16$ and $I_v = 0.04$ for (a) and $\delta = 7$ for (b)). (ii) In case that only the in-phase state is stable ($I_x = 0.2$ and $I_v = 0.1$ for (a) and $\delta = 10$ for (b)).

that the anti-phase synchronization became unstable through the Neimark-Sacker bifurcation. This result is consistent with our previous report ([30] in the main text). At $\delta \simeq 8.6$, the real part of λ_{AP} changed from negative to zero. Thus, in addition to the destabilization of the anti-phase synchronization, the disappearance of the anti-phase synchronization via the Hopf bifurcation might also occur in this system with the greater coupling strength.

VII. INFERENCE OF THE COUPLED SYSTEM USING A SINGLE TIME SERIES

The results of the inference from each single time series under the same conditions as those for the time range in the inference using all initial conditions as in Fig. 2 in the main text and Fig. S2 are exhibited in Fig. S4.